IET Generation, Transmission & Distribution

Research Article

IET Journals
The Institution of Engineering and Technology

Microgrid protection using Hilbert–Huang transform based-differential scheme

ISSN 1751-8687
Received on 10th January 2016
Revised on 16th June 2016
Accepted on 3rd July 2016
doi: 10.1049/iet-gtd.2015.1563
www.ietdl.org

Ashika Gururani[1] ✉, *Soumya R. Mohanty*[1], *Jagadish Chandra Mohanta*[2]

[1]*Department of Electrical Engineering, MNNIT, Allahabad, India*
[2]*Department of Mechanical Engineering, MNNIT, Allahabad, India*
✉ *E-mail: ashikagururani@gmail.com*

Abstract: Time–frequency-based differential scheme is proposed for microgrid protection using non-stationary signal analysis. The non-stationary signal processing algorithm Hilbert–Huang Transform (HHT) have been implemented for the protection objective and the comparative assessment with that of S-transform, differential current is carried out in order to demonstrate the reliability of the proposed protection scheme with different case studies. The series of simulation results demonstrates the efficacy of HHT, than that of S-transform in some critical cases such as high impedance fault where accurate detection is a challenge. The configuration of the microgrid test model has been developed in PSCAD with different distributed generation such as photovoltaic and wind generation system penetrated at different buses. Thus, it is found that the HHT scheme is quite reliable and efficient for fault detection objective.

1 Introduction

With the increase in energy demand and rise in climate concern the focus is on using the renewable resources or nuclear to meet out the energy requirement. The renewable energy resources consist of hydro, solar, wind, tidal, geothermal, biomass and so on. These are known as distributed generation (DG). When these DGs are employed in conjunction or more than one unit we use the term microgrid. Microgrid is a low-to-medium voltage energy network that contains DGs integrated with power electronic converter and electric storage devices with controllable loads. It can be operated in grid connected as well as in islanded mode [1, 2].

Several advantages of DG include the increase in efficiency, reduction of transmission losses, reduced greenhouse gases and pollutant emissions, enhancement of power quality, continuity, and reliability. However, the integration of these DGs to a distribution network involves a lot of technical challenges, e.g. voltage and frequency control, stability problems, steady state and transient over/under voltages at the points of connection, malfunction of protection devices, and power quality problems [3]. From the above discussed problems, microgrid protection is a major issue, which is focused in the subsequent section on the paper. The protection of microgrid becomes a major challenge because the radial nature of power flow does not prevail in the reconfigured network. As a matter of fact, the power flow becomes bidirectional and due to the wide variation in the magnitude of short circuit current both in grid connected mode and islanded mode [4–6]. In case of inverter-based distributed generators, the fault current in islanded mode is limited to twice the inverter-rated current, which may be 4–10 times if induction and synchronous DGs are present [7]. In [8–11], protection schemes which employ conventional over current relays have been proposed, but in islanded mode they will not suffice. The protection scheme of microgrid must be formulated in such a way that it ensures safe operation against all the faults in both grid connected mode and in islanded mode. In [12], protection scheme employing static switch with each DG source having its own relay is proposed. It works well for single line-to-ground and line-to-line fault, but fails to detect high impedance fault (HIF). There is another scheme which uses over current relays with voltage and frequency for backup protection [13], but this again fails to detect HIF.

The design of protection schemes using sequence components is complex and suffers from the relay coordination [7, 8]. The scheme that uses the communication-based protection in the differential scheme has the problem of time synchronisation as well as the coordination [6, 12, 14]. Further the protection scheme using voltage with undefined communication link has been proposed in [15], which is ineffective against HIF.

To overcome the limitations incurred with the techniques discussed above, the time–frequency based techniques, such as S-transform and Hilbert–Huang Transform (HHT)-based algorithm may be employed to minimise the relay coordination and time synchronisation problem. S-transform for microgrid protection in grid connected as well as in islanded mode considering both radial and loop network has been presented in [16]. However, the implemented scheme is not adaptive and may not be effective in some cases. In this paper, HHT-based scheme has been proposed and a comparison has been made with S-transform-based differential scheme. The advantage of HHT is that there are no predetermined set of functions required and it projects a non-stationary signal onto a time–frequency plane using a mono component signals, thus making it adaptive in nature [15–18].

2 Test system

A 14 bus microgrid test system as shown in Fig. 1 is modelled in PSCAD platform. It is connected to grid with rating of 50 MVA, 120 kV, and 60 Hz by means of the main transformer, T1 through Bus 1. Three DGs, i.e. a photovoltaic (PV) system and two wind systems are penetrated into the microgid system at Bus 5, Bus 10, and Bus 12, respectively. The buses were separated by a distance of 10 km by pi section distribution line. The number of relay units being employed were 21, one connected with main breaker and rest with the feeder breakers. The wind farm consists of four wind turbines and the integration in the model is tested using both synchronous and induction generator. The wind turbine is rated as 2 MW and the voltage rating in the case of synchronous generator is 0.4 kV line to neutral. The PV consists of 100 modules connected in series per array and 200 in parallel, the line to neutral voltage is 0.5 kV and the power delivered is 12 MW. The model shows the location of various relays in the system. The system

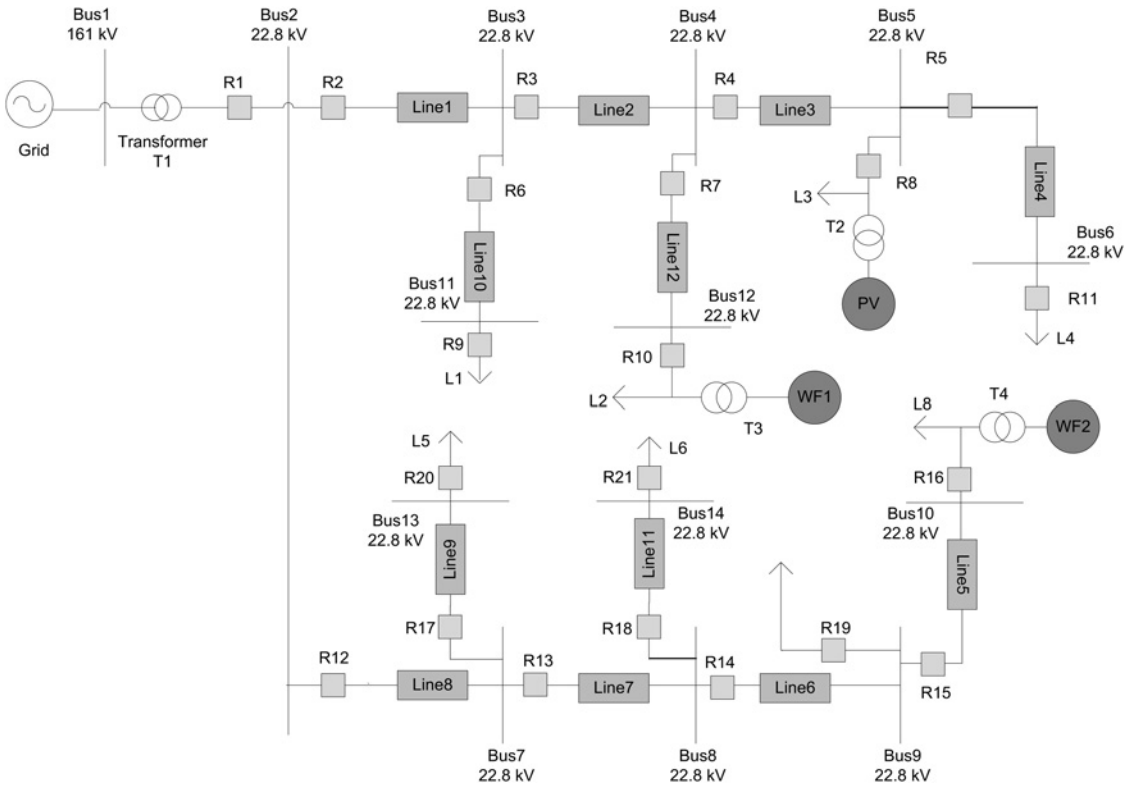

Fig. 1 *Microgrid test model*

consists of 8 loads and 21 digital relay units, one connected with main breaker and rest with feeder breakers. The current transformer ratios (A/A) at the various relays are set as 1000/1 for relay R1, 800/1 for relays R2 and R12, and 300/1 for rest of the relays.

The test system is studied in both operating modes, i.e. in grid connected mode and islanded mode. In grid connected mode, all the DG sources are present along with the utility. In islanded mode, the microgrid is disconnected from the utility grid and is powered only through DGs.

3 Methodology

The proposed technique consists of differential energy-based protection scheme using two time–frequency transforms-S-transform and HHT and comparison has been made between the two. S-transform is a time–frequency analysis method, deduced from short-time Fourier transform and continuous Wavelet transform. It is based on a scalable localising Gaussian window which has a progressive frequency dependent resolution which provides it great flexibility and utility in the processing of non-stationary signal. It is completely inter-convertible between time domain and frequency domain. It also has much better anti-noise performance than traditional methods for non-stationary signal processing. Hence, based on the superior time–frequency resolution, it can be used to describe the structure of incoming signal effectively.

The HHT is a combination of empirical mode decomposition (EMD) and Hilbert spectral analysis (HSA). It is an adaptive method applied to non-stationary and non-linear data and hence is highly efficient. The results obtained are much sharper than any of the traditional methods of time–frequency–energy representation. In the proposed technique, fault currents at both ends of the feeders are retrieved, which are then processed through transforms and then the spectral energy content is computed. The difference in energy content of time–frequency contours of the signals on the two sides indicates the fault or no-fault condition. Further, a threshold is set for detection of the fault after analysing the data considering the various cases. Extensive study of the differential energy curves was performed under the various fault conditions for setting the threshold differential energy. A tripping signal can be issued to the circuit breakers installed at the ends of the line if the differential energy exceeds this threshold. Fig. 2 shows the proposed scheme. The relays at the ends of a bus are considered and not at the ends of the line, this is because it reduces the number of relays being used and hence, the cumbersomeness because the results obtained in this case are satisfactory enough for the detection purpose. However, the circuit breakers need to be installed at the ends of the line for its isolation in case of a fault.

The threshold set is different for grid connected mode than that of islanded mode and HIF because of the variation in currents levels and hence in spectral energy. Fig. 3 shows the flow diagram of the scheme.

3.1 S-transform

S-transform is an extension of wavelet transform and short term Fourier transform (STFT). It is proposed by Stockwell and his coworkers in 1996 [19–21]. It uses scalable window, known as Gaussian window, unlike STFT that uses fixed window and hence unsuitable for non-stationary signals. It is fully convertible from time domain to frequency domain and vice versa. S-transform can be represented in terms of amplitude $A(i, n)$ and phase spectrum $\phi(i, n)$ as

$$S(i, n) = A(i, n)e^{j\phi(i,n)} \tag{1}$$

The spectral energy of the signal can be obtained by the following equation

$$E_S = [A(i, n)]^2 \tag{2}$$

3.2 Hilbert–Huang transform

The HHT is NASA's designated name and consists of EMD and HSA. The key part is the EMD which decomposes a data set into finite and smaller components called intrinsic mode functions

IET Gener. Transm. Distrib., 2016, Vol. 10, Iss. 15, pp. 3707–3716

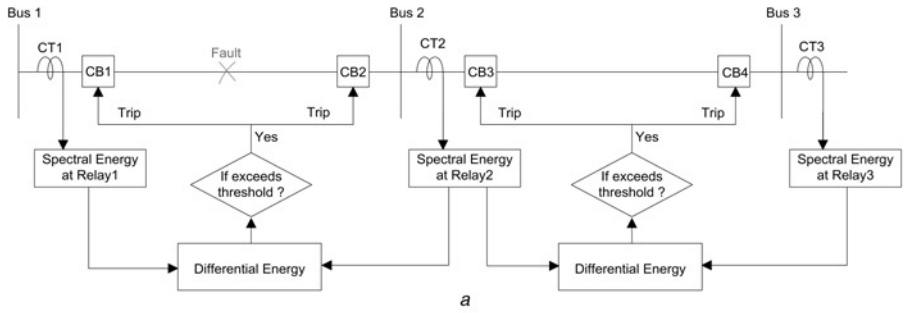

a

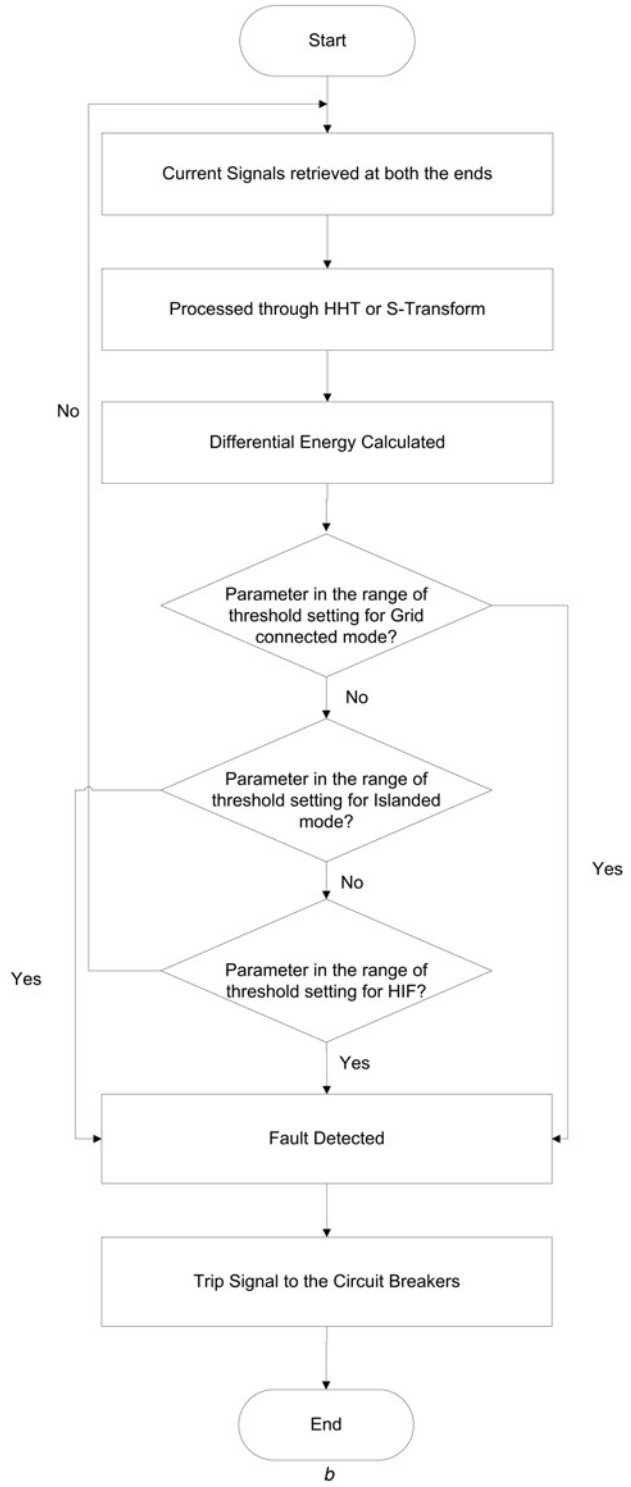

b

Fig. 2 *Tripping signal issued to the circuit breakers installed at the ends of the line if the differential energy exceeds the threshold*

a Proposed scheme
b Flow diagram of the scheme

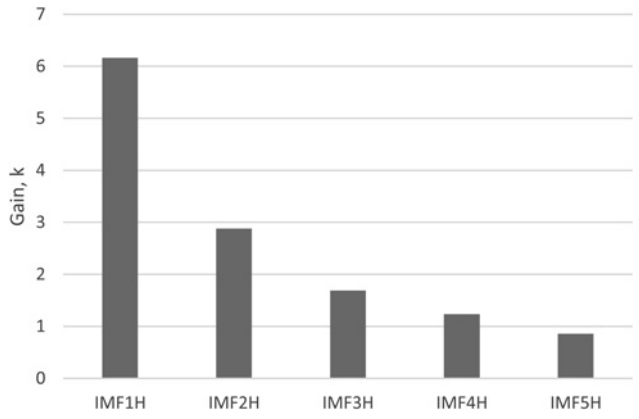

Fig. 3 *Gain, k, for Hilbert IMFs and difference of IMF1H between relays R2 and R3*

(IMFs). The Hilbert transform of these IMFs is then calculated in order to obtain the instantaneous frequencies as a function of time [18, 22–25].

3.2.1 Empirical mode decomposition: Empirical mode decomposition extracts the mono component and symmetric components from the non-linear and non-stationary signals by sifting process. Sifting is the process of removing the lowest frequency information until only the highest frequency remains. It decomposes a signal into IMFs. An IMF represents an oscillating wave if it satisfies the following two requirements:

(i) In a data set, the number of extreme and the number of zero-crossings must be either equal or differ at most by one.
(ii) At any point, the mean value of the envelope defined by the local maxima and the local minima is zero.

The decomposition of IMFs from EMD is done by the following procedure:

1. In the test data, identify the local maxima and minima and form two envelopes connecting them, respectively, with cubic splines.
2. Mean, $m(t)$ of the two envelopes is calculated. Subtracting it from the original signal $x(t)$, we get the first component, $i_1(t)$

$$i_1 = x(t) - m(t) \tag{3}$$

3. If $i_1(t)$ satisfies the above two conditions, then it is the first IMF else it is treated as the original function and steps (1)–(3) are repeated to obtain component $i_{11}(t)$ such that

$$i_{11} = i_1(t) - m_1(t) \tag{4}$$

4. After repeating sifting k times, $i_{1k}(t)$ becomes first IMF, imf_1.
5. Separate IMF1 from $x(t)$ and let it be $r_1(t)$, such that

$$r_1(t) = x(t) - \text{imf}_1 \tag{5}$$

6. $r_1(t)$ is taken as the original signal and steps (1)–(5) are repeated to obtain the second IMF.

The above procedure is repeated n times and n such IMFs are obtained. The stopping criterion for the decomposition process is when $r_n(t)$ a monotonic function becomes so that no more IMF can be extracted from it.

3.2.2 Hilbert transform: The IMFs are analytic function and for creation of instantaneous frequency of each IMF Hilbert transform is

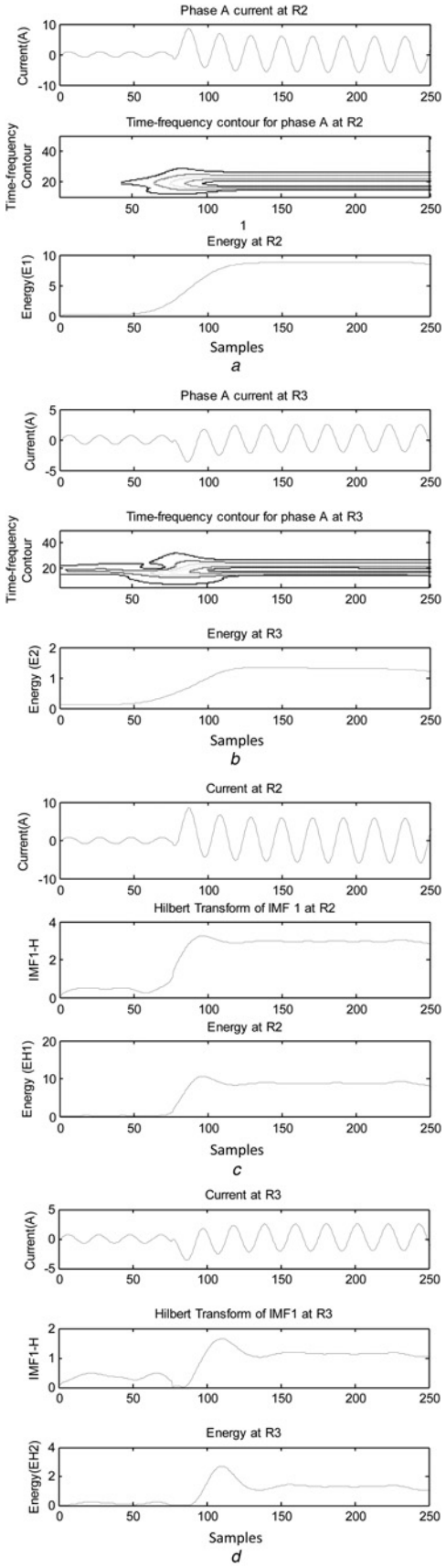

Fig. 4 *Fault current, S-transform and spectral energy of the fault current due to S-transform*

a Retrieved at R2
b Retrieved at R3; fault current, Hilbert transform of IMF1 and spectral energy of the fault current due to HHT
c Retrieved at R2
d Retrieved at R3

IET Gener. Transm. Distrib., 2016, Vol. 10, Iss. 15, pp. 3707–3716

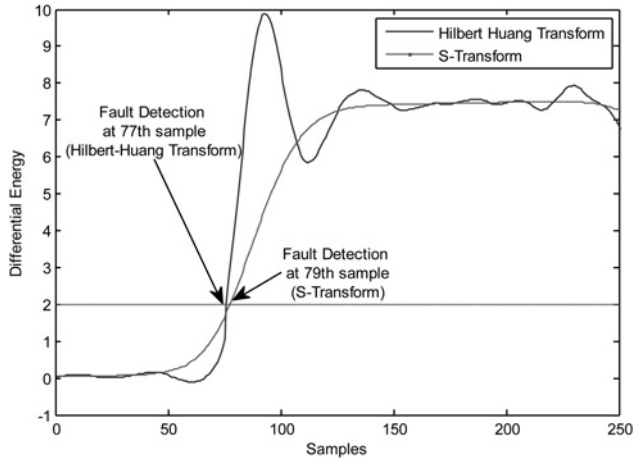

Fig. 5 *Differential energy due to S-transform and HHT with the threshold setting for LG fault on line 1*

used. The Hilbert transform of a time domain signal $x(t)$ is another time domain signal, denoted by $\hat{x}(t)$, such that $z(t) = x(t) + j\hat{x}(t)$ is an analytic signal. Magnitude $A(t)$ and phase $\theta(t)$ can be calculated as

$$A(t) = [x^2(t) + j\hat{x}2(t)]^{1/2} \tag{6}$$

$$\theta(t) = \tan^{-1}\left[\frac{\hat{x}(t)}{x(t)}\right] \tag{7}$$

Instantaneous frequency is given by the following equation

$$f_0(t) = \frac{1}{2\pi t}\tan^{-1}\left[\frac{\hat{x}(t)}{x(t)}\right] \tag{8}$$

The spectral energy of the signal can be obtained by the following equation

$$E_H = [A(t)]^2 \tag{9}$$

4 Methodology

The current signals at the various relays are retrieved. The sampling frequency was set as 1.2 kHz, i.e. 20 (1.2 k/60) samples per cycle. These signals are then subsequently processed through the S-transform and HHT. After the spectral energy content due to both the transforms had been obtained at the respective relays, the difference between the energy content was calculated between different relays. The differential energy calculated at the adjacent buses is used for fault detection by setting up of a threshold.

Out of the various IMFs obtained from the EMD, the most efficient one is found out for the fault detection with incorporation of mutual information (MI) [26] calculation between the fault and no fault conditions.

MI between two signals X and Y can be expressed as

$$I(X;\, Y) = H(X) + H(Y) - H(X,\, Y) \tag{10}$$

$$\text{where } H(X) = -\text{sum}P(X)\log[P(X)] \tag{11}$$

Here $H(X)$ and $H(Y)$ are the marginal entropies and $H(X, Y)$ is the joint entropy of X and Y, these are defined in terms of marginal probability density function $P(X)$. If X and Y are independent, then MI = 0. The signals having the least value of MI will be most distinct.

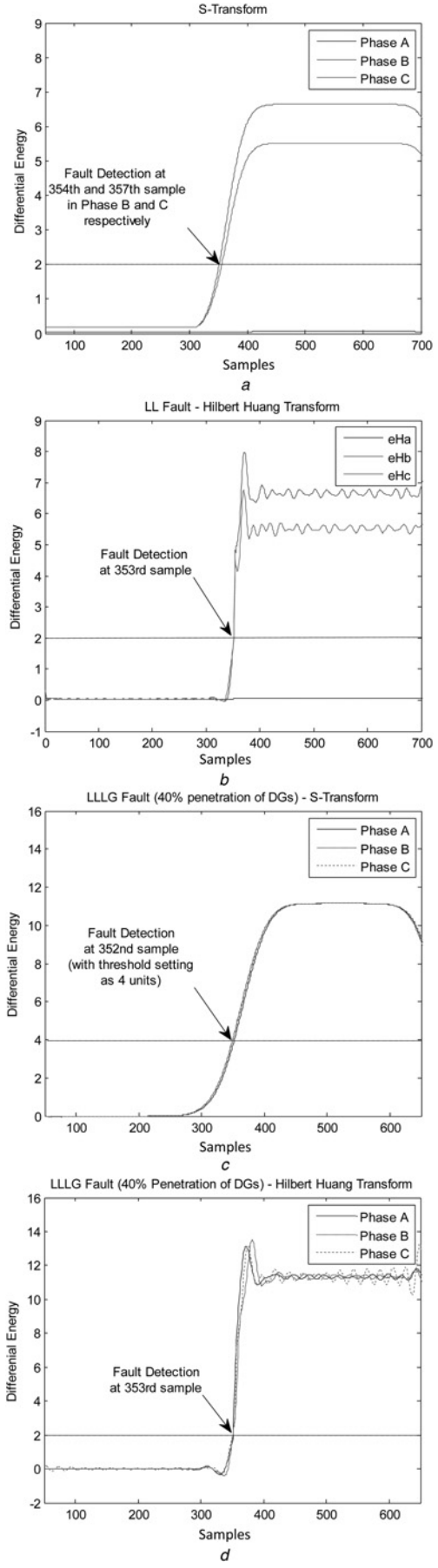

Fig. 6 *Differential energy and the threshold setting for*

a, *b* LL fault on line 6
c, *d* LLLG fault on line 7

Table 1 Effect of change in samples for different penetration level under grid connected mode

Penetration level of different DGs	Fault type	Sample at which fault occurs	HHT		S-transform	
			Threshold setting	Sample at which fault gets detected	Threshold setting	Sample at which fault gets detected
100% PV, 100% WF1, 100% WF2	LG on line 1	75	2	77	2	79
	LL on line 1	250	2	252	2	253
	LLG on line 2	250	2	252	2	252
	LLLG on line 7	350	2	351	2	352
100% PV, 80% WF1, 80% WF2	LG on line 1	350	2	353	2	354
	LL on line 1	350	2	353	2	354
	LLG on line 2	350	2	353	2	353
	LLLG on line 7	350	2	352	2	353
80% PV, 60% WF1, 60% WF2	LG on line 1	350	2	353	3	353
	LL on line 1	350	2	353	3	353
	LLG on line 2	350	2	353	3	352
	LLLG on line 7	350	2	353	3	352
40% PV, 40% WF1, 40% WF2	LG on line 1	350	2	354	4	355
	LL on line 1	350	2	354	4	354
	LLG on line 2	350	2	354	4	354
	LLLG on line 7	350	2	353	4	352

To reduce the confusion that is created by MI, gain k was defined which is the inverse of MI

$$k = \frac{1}{\text{MI}} \tag{12}$$

The IMFs having highest value of k will be most suitable for fault detection because the pattern exhibited by them will be most distinct from that during no-fault condition. Fig. 3 shows the gain k for Hilbert transforms of different IMFs. It can be seen that the gain, k, is highest in case of Hilbert transform of IMF1, 7.03, compared with that at IMF2H, 2.88, IMF3H, 1.68, IMF4H, 1.23, and IMF5H, 0.86. The value of gain is 11.40 for the difference of IMF1Hs at relay R2 and relay R3. Therefore, Hilbert transform of IMF1 can only be used for the detection of fault.

The simulation was performed considering the various cases:

- Operation of the microgrid in grid connected mode and simulating different fault conditions including HIF;
- Operation of the microgrid in islanded mode and simulating different faults;
- Effect of change in irradiance on solar panel;
- Effect of change of the wind speed;
- Performance of different generators in case of wind farm, i.e. synchronous and induction generators;
- Operation under different P reference control values;
- Changing switching frequency and modulation index of inverters;
- Simulation performed for different penetration of DGs.

5 Simulation results

5.1 Case 1: grid connected mode

The microgrid is connected with grid in this mode of operation. The simulations are performed under the various conditions and the results are then analysed for setting up of threshold. Figs. 4*a*, *b* and 5*c*, *d* depict the results for S-transform technique and HHT technique, respectively, when LG fault is simulated on line 1. The difference of the spectral energy content at relays R2 and R3 are obtained. Fig. 5 shows the two differential energies at these two relays. The fault is simulated at 75th sample and get detected by S-transform and HHT schemes at 79th and 77th sample, respectively, with the threshold set at 2.

Figs. 6*a* and *b* show the differential energy curves due to HHT and S-transform for the three phases when double line fault on phases B and C was simulated on line 6 at 350th sample with penetration level of wind farm (WF)1 and WF2 set as 80%. The differential energy is computed at relays R14 and R15. It can be seen that the differential energy of phases B and C rises and exceeds the threshold, 2, at 354th and 357th samples for phases B and C, respectively, in case of S-transform and at 353rd sample for HHT.

Figs. 6*c* and *d* show the differential energy graphs when the penetration of DGs was set to 40% for 3-phase-to-ground fault. The fault was sampled at 350th sample. It was observed that with the threshold setting set at 2 units, the fault detection was not possible in case of S-transform and threshold will have to be increased to 4 in order to detect the fault. However, on changing the threshold setting to 4 the numbers of samples after which the fault gets detected in the above two cases increases by 13 (0.65 cycles) samples in first case and 24 (1.2 cycles) and 27 (1.35 cycles) samples in second case. However, this was not the case with HHT and the fault gets detected at 353rd sample with threshold kept constant as 2.

These simulations were performed for various shunt faults at different locations and threshold 2 was found to be efficient for fault detection for all of them in case of HHT. However, it changes with the penetration level in case of S-transform. With the change in penetration level of different DGs the power output of the DG changes which leads to change in the current contributed by DGs. This change is mostly visible in case penetration level of wind turbine is changed. This is because the short circuit current contributed by wind turbine is 3–4 times the current under normal conditions, whereas this current in case of PV is limited to 1.5–2 times. Hence, changing the penetration level of PV does not affect the threshold setting. The effect of the change in penetration level is listed in Table 1.

It can be inferred that the in the case of S-transform the threshold setting has to be changed to detect the fault at the right instant. This is because the S-transform uses a window and with the decreasing level of currents the difference increases in case of fault conditions and higher threshold setting will be required for correct operation. However, this is not the problem in case of HHT and same threshold will be able to detect all type of faults and no change in relay settings will have to be made if HHT-based scheme is employed, making it more reliable.

5.2 Case 2: islanded mode

The microgrid is disconnected from the grid and now the source of generation present is only DGs. In this case, the short circuit current decreases appreciably compared with grid connected mode and therefore the same threshold setting remains no longer applicable for fault detection. Figs. 7*a* and *b* show the results for a LLLG fault simulated on line 12 at 300th sample. It was observed that the differential energy rises in negative direction for both schemes. The threshold is set at −0.3. Fig. 7*c* depicts the results when the penetration of DGs was reduced to 50%, then the fault simulated at 200th sample gets detected at 210th sample in case of HHT, i.e. after 0.5 cycles and after 249th sample, i.e. 2.45 cycles in case of S-Transform.

IET Gener. Transm. Distrib., 2016, Vol. 10, Iss. 15, pp. 3707–3716

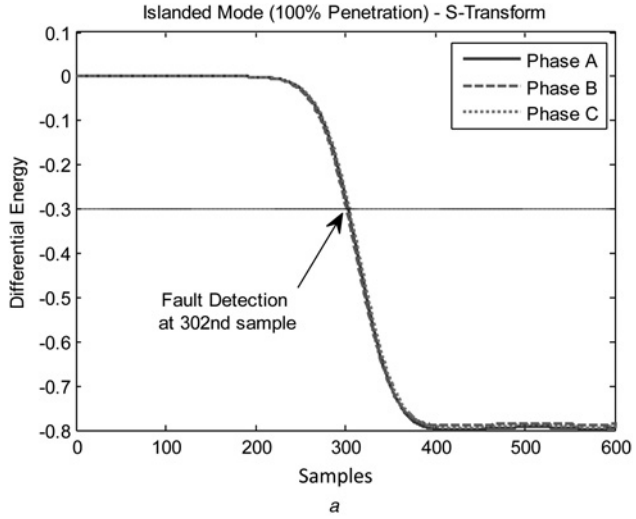

a

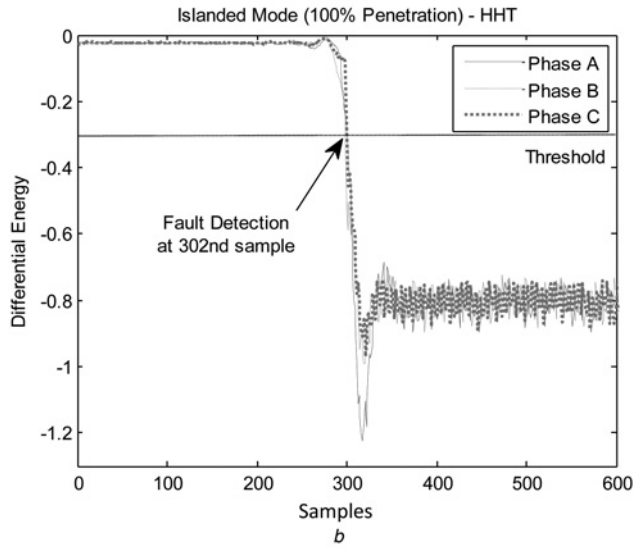

b

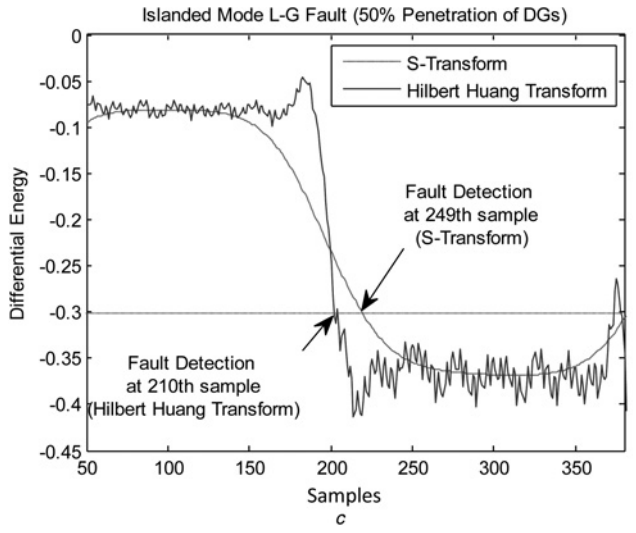

c

Fig. 7 *Differential energy for LLLG fault in islanded mode (100% DGs penetration) on line 12 due to*

a S-transform
b HHT
c Differential energy for LL fault in islanded mode (50% DGs penetration) on line 1

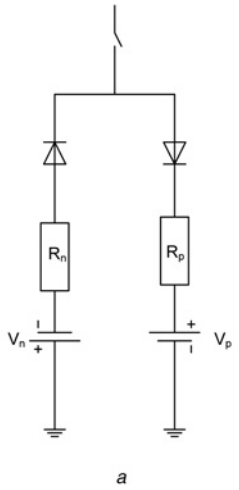

a

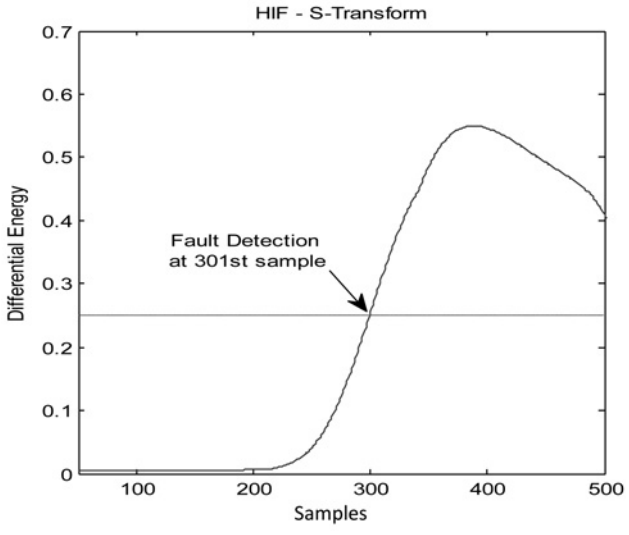

b

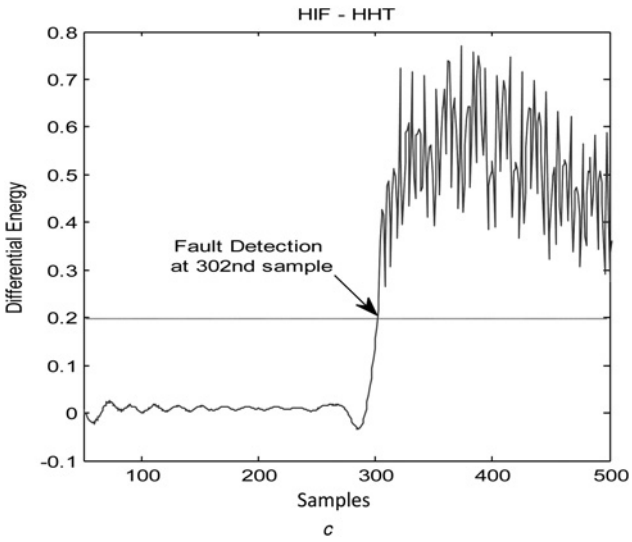

c

Fig. 8 *HIF is difficult to detect by conventional techniques and using sequence component techniques because the magnitude of fault current*

a HIF model
b Differential energy due to HHT and the threshold setting for HIF fault on line 1
c Differential energy due to S-transform and the threshold setting for HIF fault on line 1

5.3 Case 3: HIF

The HIF faults are stochastic or non-linearly deterministic in nature. Its two characteristics are- (i) low fault current and (ii) arcing. It does not necessarily involves ground and may occur when the line comes in contact with ground, road surface, sidewalk, sod, tree limb, or with some other surface [27]. They are difficult to detect by conventional techniques and using sequence component techniques because the

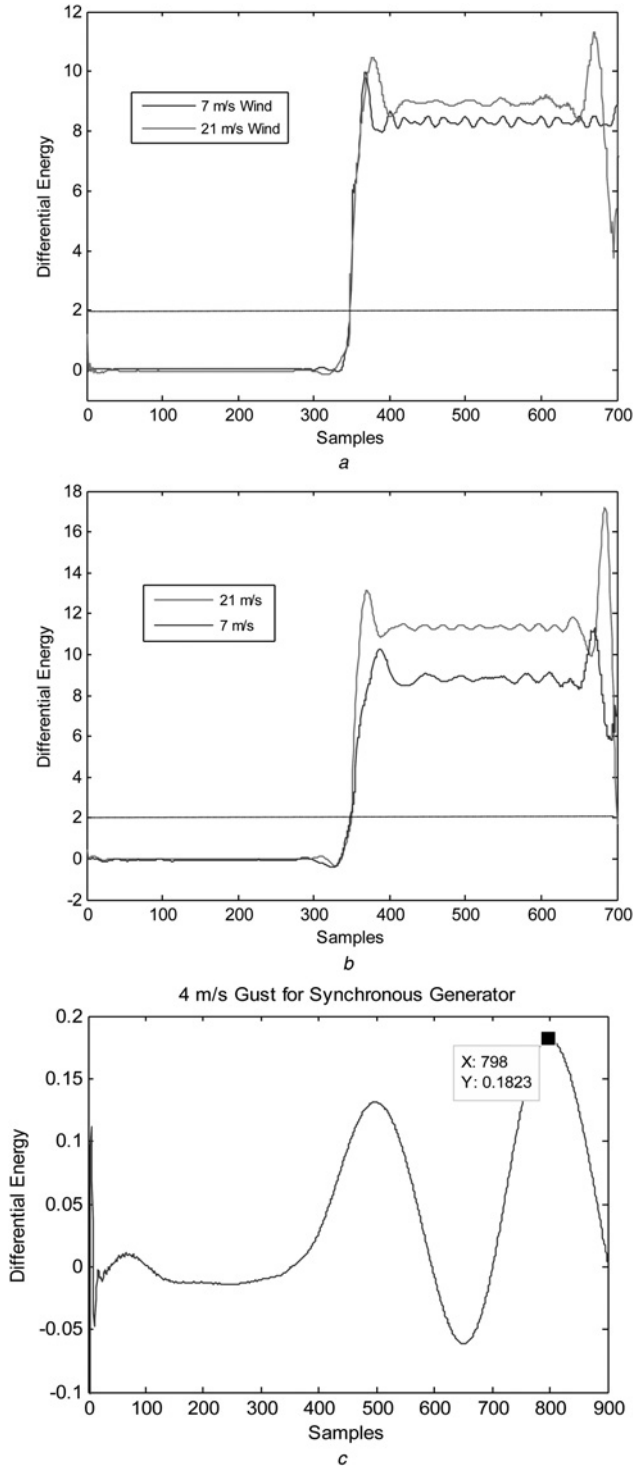

Fig. 9 *Range of operation for various parameters*

a Differential energies in case of LG fault at line 6 in case $P_{\text{Reference}}$ is set as 1 MW for wind speeds 7 and 21 m/s employing induction generator
b $P_{\text{Reference}}$ set as 3 MW
c Differential energy for synchronous generator simulating WF at 4 m/s Gust speed which occurs at 350th sample

magnitude of fault current in this case is not high enough. Its modelling is difficult and was modelled as depicted in Fig. 8*a*. Two anti-parallel diodes, resistors, and DC sources were used [16, 28]. The value of DC source was set as, $V_p = 8$ kV and $V_n = 9$ kV and the resistances were set as $R_p = 272\ \Omega$ and $R_n = 290\ \Omega$. Figs. 8*b* and *c* show the HIF fault current waveform with the

Table 2 Range of operation for different parameters

Parameters	Range of operation
change of irradiance	600–1000 W/m^2
cell temperature variation	25°–50°
wind speeds	7–21 m/s
P reference	1–3 MW
gust speed (synchronous generated employing WF)	Upto 4 m/s
carrier frequency of the PWM inverter	1080–4000Hz
modulation index of the PWM inverter	0.4–0.7

S-transform and HHT on phase A under grid connected mode on line 11. Both methods were able to detect HIF. However, different threshold levels were set for the fault detection in either cases. The threshold level in case of HHT was set as 0.2 and in case of S-transform as 0.25.

The scheme was found to be effective and yields correct results if the carrier frequency of the pulse width modulation (PWM) inverter employed in PV is varied in the range 1080–4000 Hz. Change of irradiance on the PV from 600 to 1000 W/m^2 also gives accurate results in all the cases. Cell temperature variation between 25° and 50° also does not affect the scheme. This is because the maximum output current of PV is limited to 1.5–2 pu of the rated current because of the maximum power point tracking block and the inverter.

The model is simulated for the wind speeds in the range 7–21 m/s, this is because the pitch angle controls the power output of the generator to remain within the rated limit. If the wind speed remains constant, i.e. no variation in wind is assumed, then the scheme works effectively in the entire range. However, if the wind is assumed to vary that is a gust or ramp is considered then the case is different for induction generator and synchronous generator. If induction generators were used in wind farms, then the scheme works effectively in case of speed variations and works effectively even in the presence of a gust of wind of 5 m/s. However, in case of synchronous generators it remains effective till 4 m/s gust and the maximum value of differential energy reaches 0.1823 and when the speed is further increased then the differential energy becomes comparable with the threshold setting for HIF, leading to mal-operation. It is depicted in Fig. 9*c*. The model is also found to run effectively for change in the *P* reference control between values 1 and 3 MW. However, if this *P* reference is changed when the microgrid is in operation, then the transient change in current is high enough to cause false tripping of relay. The range of operation for various parameters is shown in Table 2 and the differential energy waveform is depicted in Figs. 9*a* and *b*.

6 Discussion

The purpose of this paper is to propose a well efficient scheme for fault detection in a microgrid system. It is inferred that the differential energy using HHT scheme works effectively under both modes, i.e. grid connected and islanded. The thresholds setting for both the modes are quite different and will not interfere with other. In grid connected mode, the differential energy rises in positive direction whereas in islanded mode the rise is in negative direction this is because of the high short circuit current when connected to grid. S-transform uses the scalable Gaussian window because of which the rise in differential energy is not steep. This makes the setting of threshold difficult and it has to be set with great caution or the fault detection may get delayed. Also, this is the reason that the same threshold is not applicable for changing penetration of DGs. Thus, the relay settings have to be updated with the changing penetration level and hence, also with the changing microgrid rating. However, this is not the case with HHT as it extracts instantaneous amplitude and frequency from the current signals and is thus adaptive and more reliable. Therefore, the same relay settings are applicable for all cases. The schemes

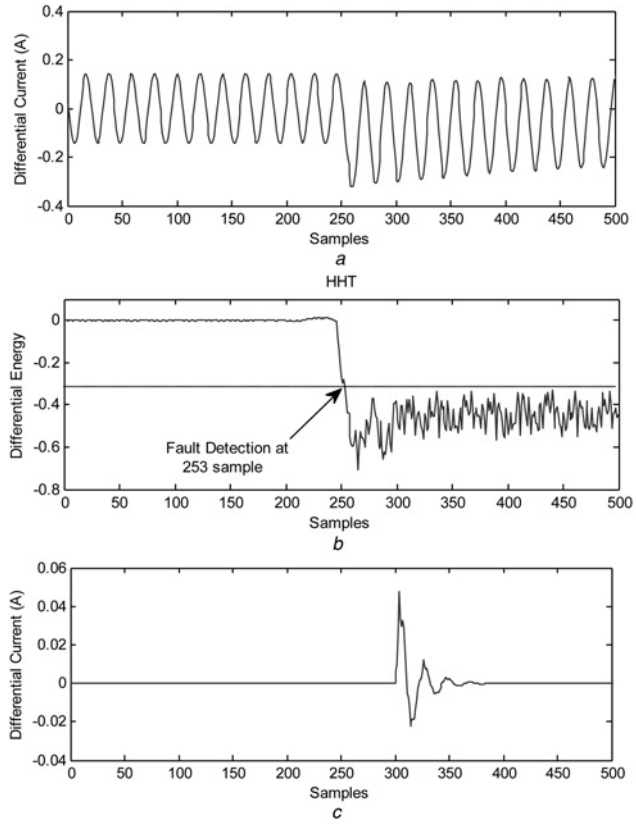

Fig. 10 *Differential current waveform for LL and HIF*

a Differential current waveform for LL fault at line 1 in islanded mode considering delay of 4.16 s

b Differential energy due to HHT for LL fault at line 1 in islanded mode considering delay of 4.16 s

c Differential current waveform for HIF fault at line 1 without considering delay

work satisfactorily for HIF faults as well in both grid connected and islanded modes, which are otherwise difficult to detect because of very low rise in current during fault. The threshold in case of HIF is set to low positive value and is quite different from the above two thresholds. For a new system the thresholds can be set by proper case study and by virtue of the comparison of various possible fault conditions.

Both the schemes as discussed in the previous paragraph have the advantage that they do not possess the problem of time synchronisation, which is one of the serious concern in case of conventional current-based schemes or sequence component-based or root mean square value of current-based schemes. The differential current waveform for LL fault at line 1 in islanded mode considering time delay of 4.16 ms in samples of R3 relay is depicted in Fig. 10*a*, it can be seen that in this case it becomes difficult to set threshold and then detect fault using conventional protection technique. However the same fault gets detected at 253rd sample using HHT-based technique as is evident from Fig. 10*b*. Fig. 10*c* shows differential current waveform during HIF fault without considering any delay. It can be seen that it becomes very difficult to detect HIF even when sampling is not considered as the amplitude is just 0.05 A and it would have become very difficult to detect using conventional techniques if time delay is considered. The differential energy waveform for the same HIF fault is shown in Fig. 8*c*. The synchronisation problem is not associated with HHT, because the energy of one cycle of cosine and sine is same and remains same even though they are shifted by 90°.Total time taken to clear the faults is the summation of the time after which the fault gets detected, time of operation of relay, and time taken in opening of circuit breaker contacts.

The HHT scheme was verified for backup protection also. In case of backup protection, the scheme suffices pretty well with the same thresholds in all the cases. However, much more extensive study can be performed for the primary and backup protection terminology so that the scheme can be applied to any practical system as the system considered in this paper does not take into account the noise at the various levels in order to simplify the calculations (See Table 3).

Table 3 Comparison of different schemes

Fault condition	Differential schemes			
Fault	S-transform	HHT	Sequence components	Differential current scheme
Grid connected mode				
LG fault	fault detected	fault detected	fault detected	fault detected
LL fault	fault detected	fault detected	fault detected	fault detected
LLG	fault detected	fault detected	fault detected	fault detected
LLLG	fault detected	fault detected	fault detected	fault detected
HIF	fault detected	fault detected	fails	fails
Islanded mode				
LG fault	fault detected	fault detected	fault detected	fails
LL fault	fault detected	fault detected	fault detected	fails
LLG	fault detected	fault detected	fault detected	fails
LLLG	fault detected	fault detected	fault detected	fails
HIF	fault detected	fault detected	fails	fails

7 Conclusion

Time–frequency-based scheme based on HHT has been discussed in this paper in the context of differential protection of microgrid. The comparative assessment of the efficacy of the proposed scheme is carried out in comparison to S-transform and differential current, sequence component as discussed in the literature. HHT-based technique is found to be more effective and reliable because it computes the instantaneous frequency of the signal and is found to work effectively under various case study as discussed in this paper. The spectral energy of the current can be computed at the two relay ends and its difference can be compared with the set threshold to identify fault scenario.

8 References

1 Lasseter, R.H.: 'Microgrids'. Proc. IEEE Power Engineering Society Winter Meeting, 2002, vol. 1, pp. 305–308

2 Oudalov, A., Fidigatti, A.: 'Adaptive network protection in microgrids', *Int. J. Distrib. Energy Source*, 2009, **4**, pp. 201–205

3 Hatziargyriou, N.D.: 'Distributed energy sources: technical challenges', *IEEE Power Eng. Soc. Winter Meet.*, 2002, **2**, (2), pp. 1017–1022

4 Sortomme, E., Mapes, G.J., Foster, B.A., *et al.*: 'Fault analysis and protection of a microgrid'. Proc. 40th North American Power Symp. (NAPS'08), pp. 1–6

5 Hussain, B., Sharkh, S., Hussain, S., *et al.*: 'Integration of distributed generation into the grid: protection challenges and solutions'. 10th IET Int. Conf. on Developments in Power System Protection, March/April 2010, pp. 1–5

6 Anil Kumar, P., Shankar, J., Nagaraju, Y.: 'Protection issues in micro grid', *Int. J. Appl. Control Electr. Electron. Eng. (IJACEEE)*, 2013, **1**, (1), pp. 19–30

7 Sortomme, E., Venkata, S.S., Mitra, J.: 'Microgrid protection using communication-assisted digital relays', *IEEE Trans. Power Deliv.*, 2010, **25**, (4), pp. 2789–2796

8 Haron, A.R., Mohamed, A., Shareef, H., *et al.*: 'Analysis and solutions of over current protection issues in a microgrid'. IEEE Int. Conf. on Power and Energy (PECon), 2012, pp. 644–649

9 Ma, J., Wanga, X., Zhang, Y., *et al.*: 'A novel adaptive current protection scheme for distribution systems with distributed generation', *Int. J. Electr. Power Energy Syst.*, 2012, **3**, (1), pp. 1460–1466

10 Wan, H., Li, K.K., Wong, K.P.: 'A multi-agent approach to protection relay coordination with distributed generators in industrial power distribution system'. Proc. Ind. Appl. Conf. 40th Ind. Appl. Soc. Annual Meeting, October 2005, pp. 830–836

11 Hadzi-Kostova, B., Styczynski, Z.: 'Network protection in distribution systems with dispersed Generation'. Proc. IEEE PES Transmission and Distribution Conf. and Exhibition, May 2006, pp. 321–326
12 Nikkhajoei, H., Lasseter, R.H.: 'Microgrid protection'. Proc. IEEE Power Engineering Society General Meeting, June 2007, pp. 1–6
13 Zeineldin, H.H., El-Saadany, E.F., Salama, M.M.A.: 'Distributed generation microgrid operation: control and protection'. Proc. Power System Conf., March 2006, pp. 105–112
14 Casagrande, E., Woon, W.L., Zeineldin, H.H., *et al.*: 'A differential sequence component protection scheme for microgrids with inverter-based distributed generators', *IEEE Trans. Smart Grid*, 2014, **5**, (1), pp. 29–37
15 Prasai, A., Du, Y., Paquette, A., *et al.*: 'Protection of meshed microgrids with communication overlay'. IEEE Energy Conversion Congress and Exposition (ECCE), 2010, pp. 64–71
16 Kar, S., Samantaray, S.R.: 'Time–frequency transform-based differential scheme for microgrid protection', *IET Gener. Transm. Distrib.*, 2014, **8**, (2), pp. 310–320
17 Ustun, T.S., Ozansoy, C., Zayegh, A.: 'Differential protection of microgrids with central protection unit support'. IEEE TENCON Spring Conf., 2013, pp. 15–19
18 Huang, N.E., Wu, Z., Long, S.R.: 'Hilbert–Huang transform', *Scholarpedia*, 2008, **3**, (7), p. 2544. Available at http://www.scholarpedia.org/article/Hilbert-Huang_transform
19 Wang, Y.H.: 'The tutorial: S transform'. Available at http://www.scholar.google.co.in/scholar_url?url=http://citeseerx.ist.psu.edu/viewdoc/download%3Fdoi%3D10.1.1.694.8727%26rep%3Drep1%26type%3Dpdf&hl=en&sa=X&scisig=AAGBfm0tO7fp7ZSvLpmrABU6948s6CMgDA&nossl=1&oi=scholarr&ved=0ahUKEwjMy_OGi63NAhUZTo8KHfoLDe4QgAMIGigAMAA
20 Sahu, S.S., Panda, G., George, N.V.: 'An improved S-transform for time–frequency analysis'. Proc. of IEEE Int. Advance Computing Conf. (IACC 2009), 2009, pp. 315–319
21 Assous, A., Boashash, B.: 'Evaluation of the modified S-transform for time–frequency synchrony analysis and source localization', *EURASIP J. Adv. Signal Process.*, 2012. Available at http://www.asp.eurasipjournals.com/content/2012/1/49
22 Tang, S., Ma, H., Su, L.: 'Filter principle of Hilbert–Huang transform and its application in time series analysis'. ICSP2006 Proc.
23 Xiao'an, Q., Xiangjun, Z., Xiaoli, Z., *et al.*: 'Traveling wave based distribution lines fault location using Hilbert–Huang transform'. Industry Applications Society Annual Meeting, 2008, IAS '08, pp. 1–5
24 Zhenghua, L.: 'Hilbert–Huang transform based application in power system fault detection'. Int. Workshop on Intelligent Systems and Applications, 2009, ISA 2009, pp. 1–4
25 Manjula, M., Mishra, S., Sarma, A.V.R.S.: 'Empirical mode decomposition based probabilistic neural network for faults classification'. Int. Conf. on Power and Energy Systems (ICPS), 2011, pp. 1–5
26 Galka, A., Ozaki, T., Yamashita, O.: 'A new approach to mutual information between pairs of time series'. Int. Symp. on Nonlinear Theory and its Applications (NOLTA 2005), 2005
27 Tengdin, J., Westfall, R., Stephan, K.: 'High impedance fault detection technology'. Report of PSRC Working Group D15
28 Zanjani, M.G.M., Karegar, H.K., Niaki, H.A., *et al.*: 'High impedance fault detection of distribution network by phasor measurement units', *Smart Grid Renew. Energy*, 2013, **4**, pp. 297–305